

Research Article

Sensitivity of Rabbit Ventricular Action Potential and Ca^{2+} Dynamics to Small Variations in Membrane Currents and Ion Diffusion Coefficients

Yuan Hung Lo,¹ Tom Peachey,² David Abramson,²
Andrew McCulloch,¹ and Anushka Michailova¹

¹ Department of Bioengineering, PFBH 241, University of California San Diego, 9500 Gilman Drive, La Jolla, CA 92093-0412, USA

² Faculty of Information Technology, Monash University, Clayton, VIC 3800, Australia

Correspondence should be addressed to Anushka Michailova; amihaylova@eng.ucsd.edu

Received 28 April 2013; Accepted 19 August 2013

Academic Editor: Jeffrey J. Saucerman

Copyright © 2013 Yuan Hung Lo et al. This is an open access article distributed under the Creative Commons Attribution License, which permits unrestricted use, distribution, and reproduction in any medium, provided the original work is properly cited.

Little is known about how small variations in ionic currents and Ca^{2+} and Na^+ diffusion coefficients impact action potential and Ca^{2+} dynamics in rabbit ventricular myocytes. We applied sensitivity analysis to quantify the sensitivity of Shannon et al. model (Biophys. J., 2004) to 5%–10% changes in currents conductance, channels distribution, and ion diffusion in rabbit ventricular cells. We found that action potential duration and Ca^{2+} peaks are *highly sensitive* to 10% increase in L-type Ca^{2+} current; *moderately influenced* by 10% increase in Na^+ - Ca^{2+} exchanger, Na^+ - K^+ pump, rapid delayed and slow transient outward K^+ currents, and Cl^- background current; *insensitive* to 10% increases in all other ionic currents and sarcoplasmic reticulum Ca^{2+} fluxes. Cell electrical activity is strongly affected by 5% shift of L-type Ca^{2+} channels and Na^+ - Ca^{2+} exchanger in between junctional and submembrane spaces while Ca^{2+} -activated Cl^- -channel redistribution has the modest effect. Small changes in submembrane and cytosolic diffusion coefficients for Ca^{2+} , but not in Na^+ transfer, may alter notably myocyte contraction. Our studies highlight the need for more precise measurements and further extending and testing of the Shannon et al. model. Our results demonstrate usefulness of sensitivity analysis to identify specific knowledge gaps and controversies related to ventricular cell electrophysiology and Ca^{2+} signaling.

1. Introduction

Several ionic models have been developed to investigate the subcellular mechanisms regulating excitation-contraction coupling (ECC) in rabbit ventricular cardiomyocytes [1–7]. In 2004, Shannon and colleagues published a detailed model for Ca^{2+} handling and ionic current that accurately represents sarcoplasmic reticulum (SR) Ca^{2+} -dependent release and simulates basic ECC phenomena. This model was the first to include (1) the subsarcolemmal Ca^{2+} compartment to the other two commonly formulated cytosolic Ca^{2+} compartments (junctional and bulk, [8]), (2) the variations in the locations of ion transporters throughout the cell surface membrane, (3) Ca^{2+} and Na^+ transport between the subcellular compartments, and (4) Na^+ buffering inside. Latest studies extended further the Shannon et al. ionic model in

rabbit ventricular cells. Mahajan and colleagues modified L-type Ca^{2+} current and Ca^{2+} cycling formulations, based on new experimental patch-clamp data, and used the updated model to investigate the mechanisms regulating ventricular tachycardia and fibrillation [4, 5]. Morotti et al. improved Mahajan's et al. model of rabbit ventricular I_{Ca} and examined the relative contributions of voltage- and Ca^{2+} -dependent inactivation to total current inactivation [7]. Aslanidi et al. determined the functional role of each ionic channel current in modulating the action potential (AP) shape from different locations in rabbit ventricular wall [6]. Recently, using parameter sensitive analysis, Romero et al. [9] identified also key subcellular factors involved in the electrical signal generation and Ca^{2+} signal regulation in two rabbit cell models [1, 4]. Systematically characterizing AP properties, Ca^{2+} and Na^+ dynamics, and their rate dependence on

$\pm 15\%$, ± 30 , and $\pm 45\%$ variations in the main transmembrane currents' conductance they found that APD is significantly modified by most repolarization currents and that steady-state Ca^{2+} levels are strongly dependent on I_{Ca} , I_{NCX} , and I_{NaK} currents. Important limitation of these "common pool models", however, is that the subcellular compartment geometries (junctional cleft, submembrane space, cytosol, and SR) were simplified to allow prediction of total Ca^{2+} concentration ($[\text{Ca}](t)$) in the compartment of interest only.

A few reaction-diffusion models that seek to incorporate the effects of idealistic or more realistic subcellular and whole-cell geometries and to compute the spatial distributions of $[\text{Ca}]$ in cardiac, skeletal or smooth muscle cells have been published also [10–19]. Recently, the contributions of structural heterogeneities to local and global Ca^{2+} signals in rabbit ventricular myocytes with realistic t -tubule microanatomy have been investigated [20]. Limitations of these spatial models, due to complexities, are that the cell electrophysiology was simplified, the AP dynamics was not reproduced, and the effects of intracellular Na^{2+} diffusion and buffering on ECC were not investigated.

Taken together the published computational models have provided important insights into the underlying mechanisms regulating intracellular Ca^{2+} dynamics and electrophysiological behavior in rabbit ventricular cells under control and certain pathological conditions. It remains, however, poorly understood how small variations in ion currents conductance and distribution and small changes in Ca^{2+} and Na^{+} transport between cellular subdomains affect important cellular biomarkers (i.e., AP shape, $[\text{Ca}]_i$, $[\text{Ca}]_{\text{SL}}$, and $[\text{Ca}]_{\text{Jct}}$). In this study, we applied sensitivity analysis and used parameter estimation tools to investigate these questions. The sensitivity of each biomarker to 5%–10% changes in ionic currents properties and Ca^{2+} and Na^{+} diffusion coefficients were quantified using the Shannon et al. model. Validation of simulation results was performed by a comparison to experimental data in rabbit ventricular myocytes. This study identifies new experimental data required for better understanding of rabbit's electrophysiology and demonstrates the importance of sensitivity analysis as a powerful method for systematic and in-depth validation of AP models.

2. Methods

2.1. Electrophysiological Model in Rabbit Ventricular Myocytes. A diagram describing the arrangement of subcellular compartments, ionic currents and pumps, and intracellular Ca^{2+} fluxes included in the Shannon et al. electrophysiological model is shown in Figure 1.

The Shannon et al. model was adopted without changes and recent MatLab version of the code has been uploaded (<http://somapp.ucdavis.edu/Pharmacology/bers/>). The model behavior at 1 Hz pacing frequency is consistent with experimental measurements for AP-shape and global cytosolic Ca^{2+} concentrations ($[\text{Ca}]_i$) changes under control conditions [1].

2.2. Sensitivity Analysis Tools. Recently, several sensitivity analysis and parameter estimation tools and methodologies

have been developed with a specific aim to assess the robustness of the cardiac cell models' parameters, including (1) the parameter variability analysis which examine the effects of varying one parameter in time [21], (2) techniques which assess the significance of parameters using multivariable regression over randomized set of input parameters values [22], and (3) global sensitivity analysis tool which implements the Morris screening algorithm [23] within the Nimrod platform [24]. In this study, we explored two methodologies [22, 23] and compared each method potential in evaluating parameter-output correlations in the Shannon et al. electrophysiological model.

2.2.1. Partial Least Squares (PLS) Regression. PLS is a statistical method that creates a linear regression model to predict a set of dependent variables (i.e., model outputs) from a set of independent variables (i.e., model inputs) [22, 25]. PLS is particularly useful when inputs are highly correlated (i.e., multicollinear) and when there are more inputs than outputs. In regression analysis, if two highly correlated effects are measured, the more dominant effect will falsely enhance the weaker effect, leading to inaccurate sensitivity information, and misinform truly significant parameter effects [25]. Since PLS retains good predictive power when working with multicollinear data, myocyte models containing multiple correlated variables can be analyzed using PLS.

2.2.2. Nimrod Tool Family. *Nimrod* uses a simple declarative modeling language to define parametric experiments, and it automates the tasks of formulating, running, monitoring, and collecting results from multiple individual experiments. *Nimrod* is not a single tool. It incorporates *Nimrod/G*, component that distributes computations to the recourses [24, 26]; *Nimrod/O*, a component that searches for "good" solutions using nonlinear optimization algorithms [27]; *Nimrod/E*, component that helps evaluating which parameter settings are important using the experimental design [28]. *Nimrod/G* is designed to assist scientists in performing studies, using concurrent execution on a cluster of processors or the resources of a computational grid. The user prepares a "plan file" which specifies the experiment [24]. A plan file is expanded into a "run file" which lists the appropriate parameter combinations required for execution. The *Nimrod/G* core runs on a processor called the "root node" whereas individual jobs are executed on "remote nodes." *Nimrod/G* handles the file transfers required for the remote nodes, execution of computational tasks, and transfer of results back to the root node. The number of concurrent jobs is limited only by the number of processors available. Thus the user may achieve high concurrency without modifying the executables and without concern for grid specific details. *Nimrod/O* optimizes the numerical outputs of computational models. It provides a range of optimization algorithms and leverages *Nimrod/G* to perform batches of concurrent evaluations. The user prepares a "schedule file," which, like the *Nimrod/G* plan file, specifies the parameters, their ranges, and the tasks required for execution of the model. But it also specifies the optimization algorithms to be used and the settings for the algorithms.

TABLE 1: Maximal conductance varied in the model.

	Definition	Symbol	Baseline value
1	Maximal Na^+ conductance	G_{Na}	16 mS/ μF
2	Background Na^+ conductance	G_{Nab} (G_{NaBk})	$0.297 \cdot 10^{-3}$ mS/ μF
3	Maximal rapid delayed rectifier K^+ conductance	G_{Kr} (G_{IKr})	0.07 mS/ μF
4	Maximal slow delayed rectifier K^+ conductance	G_{Ks}	0.013 mS/ μF
5	Maximal fast transient outward K^+ conductance	$G_{\text{to},f}$	0.06 mS/ μF
6	Maximal slow transient outward K^+ conductance	G_{to} ($G_{\text{to},s}$)	0.02 mS/ μF
7	Maximal inward rectifier K^+ conductance	G_{KI}	0.9 mS/ μF
8	Maximal Ca -activated Cl^- conductance	$G_{\text{Cl}(\text{Ca})}$	0.109625 mS/ μF
9	Background Cl^- conductance	G_{ClBk}	0.009 mS/ μF
10	Maximal permeability of L-type Ca^{2+} channel for Ca^{2+}	P_{CaL} (P_{Ca})	$5.4 \cdot 10^{-4}$ cm/s
11	Maximal permeability of L-type Ca^{2+} channel for Na^+	P_{CaNa} (P_{Na})	$1.5 \cdot 10^{-8}$ cm/s
12	Maximal permeability of L-type Ca^{2+} channel for K^+	P_{CaK} (P_{K})	$2.7 \cdot 10^{-7}$ cm/s
13	Background Ca^{2+} conductance	G_{Cab} (G_{CaBk})	0.0002513 mS/ μF
14	Maximal Na^+ - Ca^{2+} exchange current	K_{NCX} (\bar{I}_{NCX})	9 A/F
15	Maximal sarcolemmal Ca^{2+} pump current	K_{pCa} (\bar{I}_{SLCaP})	0.0673 A/F
16	Maximal Na^+ - K^+ pump current	K_{NaK} (\bar{I}_{NaK})	1.91 A/F
17	SR Ca^{2+} release scaling factor	K_{rel} (k_s)	25 ms^{-1}
18	Maximal rate of SR Ca^{2+} uptake (SERCA)	K_{up} (\bar{I}_{SRCaP})	$5.3 \cdot 10^{-3}$ mM/ms
19	Passive SR Ca^{2+} leak scaling factor	K_{leak} (K_{SRleak})	$5.348 \cdot 10^{-6}$ ms^{-1}

Note: notations in brackets, for example, (...), show corresponding notations of some parameters used in Shannon et al. article [1]. The baseline conductance values used in this study are the same as in [1].

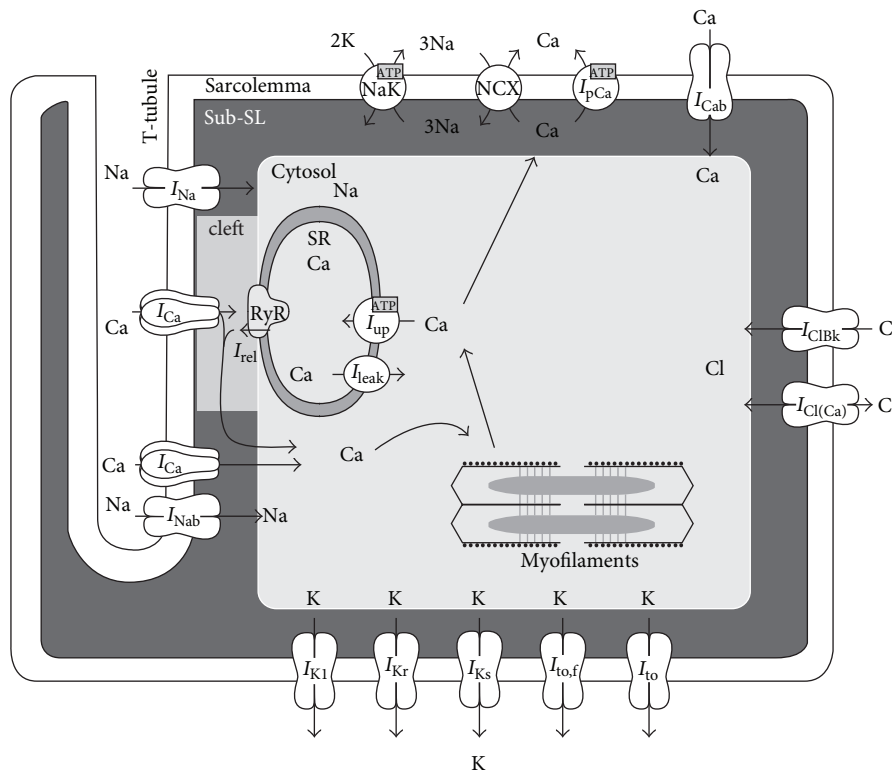


FIGURE 1: Schematic diagram illustrating the four subcellular compartments, electrophysiology, and Ca^{2+} dynamics in the Shannon et al. model in rabbit ventricular myocytes [1]. See Glossary and Tables 1–3 for the notations of the parameters used throughout the study.

TABLE 2: Fractions of total “ j ” flux varied in the model.

	Definition	Symbol	Baseline value
1	Fraction of total Na^+ current in junctional cleft	$Fx_{\text{Na(jct)}}$	0.11
2	Fraction of total background Na^+ current in junctional cleft	$Fx_{\text{NaBk(jct)}}$	0.11
3	Fraction of total Na^+ - K^+ current in junctional cleft	$Fx_{\text{NaK(jct)}}$	0.11
4	Fraction of total slow delayed rectifier K^+ current in junctional cleft	$Fx_{\text{Ks(jct)}}$	0.11
5	Fraction of total Ca-activated Cl^- current in junctional cleft	$Fx_{\text{Cl(Ca)(jct)}}$	0.11
6	Fraction of total Ca-dependent L-type Ca^{2+} current in junctional cleft	$Fx_{\text{CaL(jct)}}$	0.9
7	Fraction of total background Ca^{2+} current in junctional cleft	$Fx_{\text{CaBk(jct)}}$	0.11
8	Fraction of total Na^+ - Ca^{2+} current in junctional cleft	$Fx_{\text{NCX(jct)}}$	0.11
9	Fraction of total sarcolemmal Ca^{2+} pump current in junctional cleft	$Fx_{\text{SLCaP(jct)}}$	0.11

Notes: fraction of total j flux in SL ($Fx_{j(\text{SL})} = 1 - Fx_{j(\text{jct})}$). In the Shannon et al. article [1] $Fx_{\text{Cl(jct)}}$ corresponds to $Fx_{\text{Cl(Ca)(jct)}}$. The baseline total “ j ” flux fraction values used in this study are the same as in [1].

TABLE 3: Diffusion coefficients varied in the model.

	Definition	Symbol	Baseline value
1	Diffusion coefficient for Ca^{2+} from junctional cleft to SL compartment	$D_{\text{Ca(jct-SL)}}$	$1.64 \cdot 10^{-6} \text{ cm}^2/\text{s}$
2	Diffusion coefficient for Ca^{2+} from SL compartment to bulk cytosol	$D_{\text{Ca(SL-i)}}$	$1.22 \cdot 10^{-6} \text{ cm}^2/\text{s}$
3	Diffusion coefficient for Na^+ from junctional cleft to SL compartment	$D_{\text{Na(jct-SL)}}$	$1.09 \cdot 10^{-5} \text{ cm}^2/\text{s}$
4	Diffusion coefficient for Na^+ from SL compartment to bulk cytosol	$D_{\text{Na(SL-i)}}$	$1.79 \cdot 10^{-6} \text{ cm}^2/\text{s}$

Notes: in the Shannon et al. article [1] $D_{\text{Ca(junction-SL)}}$ corresponds to $D_{\text{Ca(jct-SL)}}$, $D_{\text{Ca(SL-cytosol)}}$ to $D_{\text{Ca(SL-i)}}$, $D_{\text{Na(junction-SL)}}$ to $D_{\text{Na(jct-SL)}}$, and $D_{\text{Na(SL-cytosol)}}$ to $D_{\text{Na(SL-i)}}$. The baseline diffusion coefficients values used in this study are the same as in [1].

Nimrod/O performs multiple searches for an algorithm and multiple algorithms, all in parallel.

2.2.3. Nimrod/E and Fractional-Factorial Design (FFD). It is often of interest for researchers to identify variable interactions because they may provide physiological insights into cell dynamics. While colinearity in multiple linear regressions is problematic and can lead to inaccurate predictions, Nimrod/E is able to circumvent this problem and successfully identify both main effects and multifactor interactions [28]. Similar to PLSR, FFD attempts to create a linear model to explain the data generated from the model; it measures and ranks main effects and two-level interactions of input variables with outputs via experimental design. However, the method chooses only those jobs that generate the most significant results by ignoring high-level interactions with little influence, thereby saving a lot of computation time. From the resulting linear model effect coefficients can also be extracted that tells the correlation between parameters and model outputs. For more complete view of successes and failures in modeling pursuits of Nimrod toolsets, refer to Abramson and colleagues papers [24, 26–28].

2.3. Parameter Sensitivity Analysis. To perform sensitivity analysis, the Shannon et al. MatLab code was modified to extract the desired model outputs. Under basal conditions or by varying one parameter at a time AP and Ca^{2+} transients appeared stable (after 6–8 s until 8 min) at stimulus frequency of 1 Hz. For this reason we recorded and analyzed AP and Ca^{2+} signals ($[\text{Ca}]_i$, $[\text{Ca}]_{\text{SL}}$, $[\text{Ca}]_{\text{jct}}$) at 9–10 s of every simulation. In all numerical experiments ($0 \leq t \leq 8 \text{ min}$) $[\text{K}]_i$

remained unchanged while the variations in $[\text{Na}]_i$ were small (ranging from $20 \mu\text{M}$ to $100 \mu\text{M}$) with insignificant effects on calculated AP and Ca^{2+} traces at 6–8 s. The APD_{60} and delta $[\text{Ca}]_j$ ($\Delta[\text{Ca}]_j$, $j = i, \text{SL}, \text{jct}$) quantities were used to analyze the model sensitivity. $\Delta[\text{Ca}]_j$ is defined as the difference between peak Ca^{2+} concentration in the particular compartment and the diastolic Ca^{2+} concentration of $0.1 \mu\text{M}$. The modified code was uploaded onto Nimrod/E toolset and was executed repeatedly using permutations of parameter sets that were $\pm 10\%$ or $\pm 5\%$ of default values (see the appendix, Tables 1–3). Then Nimrod/E fractional-factorial analysis and PLS were used to analyze the effects of single parameter changes. In addition, Nimrod/E allowed examining the two-level parameter interactions on model outputs. In the Results section the sensitivities of selected biomarkers to variations of parameters are displayed graphically as either “*Lenth plots*” in Nimrod/E, or as “*bar plots*” in PLS. Before performing PLS regression analysis to obtain sensitivity values, z -scores of input and output matrices were calculated using MatLab’s z -score function; that is, $z = (x - \text{mean}(x))/\text{std}(x)$. Each z -score value was computed using the mean and standard deviations along each column of the matrices. The columns of matrices have mean zero and standard deviation one. The PLS regression coefficients, or sensitivity values (see Figures 2, 4, and 6), indicate how changes in input parameters lead to changes in outputs. Examining these numbers allows for an assessment of the relative contributions of the various parameters. The sensitivity values in the “*bar plots*” could be interpreted quantitatively as follows. Because input and output matrices are mean-centered and normalized to standard deviations computed column by column, each sensitivity value is defined relatively to the relevant deviations. For

instance, if the regression coefficient for the input P_{CaL} and the output APD_{60} is 0.5, then when P_{CaL} is one standard deviation greater than the mean, APD_{60} will increase by half a standard deviation. Conversely, if the value is -0.5 , then when P_{CaL} is one standard deviation greater than the mean, APD_{60} will decrease by half a standard deviation, and vice versa. The *estimate* values in the “Lenth plots” (y-axis) provide a qualitative overview of the inputs’ relative effects on outputs and offer a comparison to the PLS-bar graphs. Changing the number of parameters studied slightly varied the magnitude of “regression coefficients” of bar plot and “estimate” of Lenth plot, but the relative effects and overall parameter-to-output relationships remained constant. The effects of sample sizes on model predictive efficacy by randomly picking subsets from sample pool, ranging from 15, 20, 50, 100, 200, and 500 to 1000 trials was examined. The adjusted R^2 values (*coefficient of determination, quantifying the explanatory capacity of the regression analysis*) were calculated and averaged. At the low end of 15 samples, the regression model explained $90.8 \pm 2.4\%$ of the variance. At the high end of 1000 samples, the model explained $96.4 \pm 0.3\%$ of the variance. This relatively low decrease in prediction efficacy suggests that sample sizes do not significantly change the qualitative information obtained from the experiments. Considering this statistical analysis, the results were not included.

3. Results

3.1. Effects of 10% Changes in Channels Conductances on AP Morphology and Intracellular Ca^{2+} Dynamics. Figure 2 shows the effects of 10% changes in 19 default ion channel conductances and permeabilities (see the appendix, Table 1). Both PLS and Nimrod/E methods yielded consistent results with respect to single parameter’s changes on the model outputs (APD_{60} , $\Delta[Ca]_i$, $\Delta[Ca]_{SL}$, $\Delta[Ca]_{jct}$).

The increase in L-type Ca^{2+} channel permeability (P_{CaL}) had the most pronounced effects on APD_{60} and Ca^{2+} signals, by increasing action potential duration and enhancing maximum Ca^{2+} peaks. The effects of G_{Kr} , G_{to} , and K_{NCX} , while less pronounced than P_{CaL} , were still significant. Figure 2 also shows that 10% increases in G_{Kr} and G_{to} decreased APD_{60} and Ca^{2+} peaks while 10% increase in K_{NCX} decreased Ca^{2+} peaks but increased APD_{60} . The increase in maximal NaK pump rate (K_{NaK}) had still detectable but minor effect, by decreasing both APD_{60} and Ca^{2+} peaks. The changes in SR parameters (K_{rel} , K_{up} , and K_{leak}) by 10% had negligible effects on APD_{60} and $\Delta[Ca]_i$ whereas the submembrane and junctional Ca^{2+} peaks (e.g., $\Delta[Ca]_{SL}$ and $\Delta[Ca]_{jct}$) were most affected. Figure 2 shows that 10% increases in K_{rel} and K_{up} increased $\Delta[Ca]_{SL}$ and $\Delta[Ca]_{jct}$ while K_{leak} had the opposite effect. Interestingly, 10% increase in background Cl^- conductance (G_{ClBk}) showed similar magnitude as G_{Kr} and G_{to} and demonstrated the same effects in decreasing APD_{60} and Ca^{2+} peaks. Furthermore, Nimrod/E had the advantage in predicting how 10% increases in two-parameter group can affect the model outputs. Nimrod/E predicts here that P_{CaL} and K_{NCX} combined, as well all other two-parameter group

combinations (not shown in Figure 2), had slight or no effect on the selected cellular biomarkers (APD_{60} , $\Delta[Ca]_i$, $\Delta[Ca]_{SL}$, and $\Delta[Ca]_{jct}$). The plots in Figure 3 confirm further the specific, quantitative predictions made by PLS and Nimrod/E for the effects of 10% increases in P_{CaL} , K_{NCX} , G_{Kr} , G_{to} , K_{NaK} , and G_{ClBk} on AP morphology and Ca^{2+} transients.

3.2. Effects of Changes in Membrane Transporter Distributions on AP Morphology and Intracellular Ca^{2+} Dynamics. In Shannon et al. model, cell was separated into four lumped compartments (see Figure 1): the junctional cleft (0.077% of total cell volume assuming 11% of the surface membrane junctional), the subsarcolemmal space (2% of total cell volume assuming 89% of the membrane nonjunctional) the bulk cytosol space (65% of total cell volume with remainder of the volume accounted for by mitochondria) and the SR (3.5% of total cell volume). The L-type Ca^{2+} channels were assumed concentrated within the junctional membrane such that 90% of total number were located there while all other membrane transporters (Na^+ channels, Na^+ leak, Na^+/K^+ pump, slow delayed rectified K^+ channel, Ca^{2+} activated Cl^- channel, Ca^{2+} leak, Na^+/Ca^{2+} exchanger, and sarcolemmal Ca^{2+} pump) were considered evenly distributed across the sarcolemma with 11% in the junctional cleft and 89% in the subsarcolemmal compartment [1].

To examine how the changes in ion transporter distributions affect the selected cellular biomarkers (APD_{60} , $\Delta[Ca]_i$, $\Delta[Ca]_{SL}$, and $\Delta[Ca]_{jct}$), we performed systematic analysis, increasing by 5% the basic $Fx_{j(jct)}$ while decreasing $Fx_{j(SL)}$ to keep total number of transporter protein complexes within the sarcolemma unchanged; that is, $Fx_{j(jct)} + Fx_{j(SL)} = 1$ (the appendix, Table 2). Figure 4 shows that PLS and Nimrod/E analysis again showed consistent results. The 5% increase in L-type Ca^{2+} channels fraction in the junctional cleft ($Fx_{CaL(jct)} = 0.945$) had the most pronounced effect on the model outputs, decreasing APD_{60} and Ca^{2+} peaks. The results also suggest that 5% increase in the junctional Na^+-Ca^{2+} current ($Fx_{NCX(jct)} = 0.1155$) prolonged APD_{60} while slightly affected Ca^{2+} peaks in the junctional cleft and subsarcolemmal and bulk cytosol compartments. The 5% increase in the junctional $Cl(Ca)$ ($Fx_{Cl(Ca)(jct)} = 0.1155$) had similar effect on all model outputs as the increase in $Fx_{CaL(jct)}$ but with much smaller magnitude. Results in Lenth plot (Figure 4) for the four model outputs reveal that “ $Fx_{NCX(jct)}Fx_{CaL(jct)}$ combination” as well all other two-parameter combinations had insignificant impact (not shown in Figure 4). Additional analysis of the data has been done by increasing each $Fx_{j(jct)}$ by 5% and decreasing $Fx_{j(SL)}$ ($j = CaL, NCX, Cl(Ca)$) while keeping all other model parameters constant. The results in Figure 5 confirm the predictions made by both PLS and Nimrod/E methods.

3.3. Effects of 10% Changes in Diffusion Constants on AP Morphology and Intracellular Ca^{2+} Dynamics. The effects of changes in default parameters describing Ca^{2+} and Na^+ diffusion between junctional and subsarcolemmal compartments and between subsarcolemmal and bulk compartments were

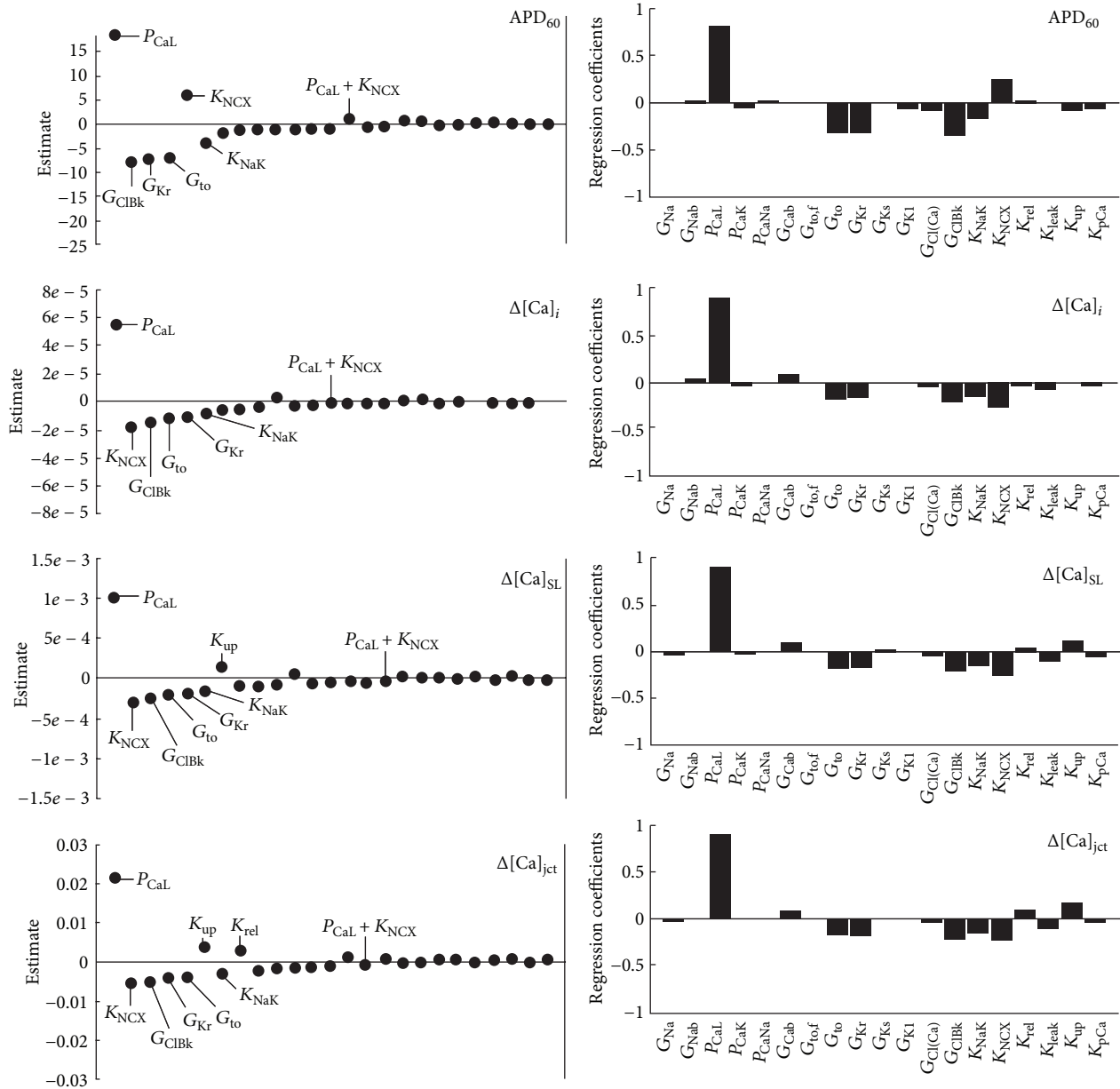


FIGURE 2: Parameter sensitivity analysis of APD_{60} , $\Delta[Ca]_i$, $\Delta[Ca]_{SL}$, and $\Delta[Ca]_{jct}$ sensitivities toward 10% increases in maximal transporters' conductance and permeability. Positive value indicates direct relationship between parameter and output (e.g., enhanced L-type Ca^{2+} permeability prolongs APD_{60}), and negative value indicates indirect relationship between parameter and output. Nimrod/E-Lenth plots (left column), PLS-bar plots (right column). Nimrod/E analysis produced similar qualitative results as PLS analysis.

also analyzed in this study (the appendix, Table 3). Figure 6 shows that 10% increases in basal $D_{Ca(jct-SL)}$ altered all model outputs, prolonging APD_{60} and increasing $\Delta[Ca]_i$ and $\Delta[Ca]_{SL}$ but decreasing $\Delta[Ca]_{jct}$. Moreover 10% increases in basal $D_{Ca(SL-i)}$ value shortened APD_{60} and increased $\Delta[Ca]_i$, $\Delta[Ca]_{jct}$, and $\Delta[Ca]_{SL}$. Interestingly, 10% increases in basal $D_{Na(jct-SL)}$ and $D_{Na(SL-i)}$ values in all three compartments had no effect on APD_{60} and Ca^{2+} peaks. Nimrod/E analysis also suggests that two-level interaction between $D_{Ca(jct-SL)}$ and $D_{Ca(SL-i)}$ had a minor effect on increasing $\Delta[Ca]_i$ while APD_{60} , $\Delta[Ca]_{SL}$, and $\Delta[Ca]_{jct}$ were unaffected. Figure 7

additionally confirms the PLS and Nimrod/E predictions for the effects of 10% increases in $D_{Ca(jct-SL)}$ and $D_{Ca(SL-i)}$ on AP morphology and Ca^{2+} transients.

4. Discussion

The main goal of this study was to perform a systematic investigation on how small variations in ionic currents and Ca^{2+} and Na^{+} diffusion coefficients modulate ventricular myocyte electrophysiology and Ca^{2+} dynamics in rabbit ventricular myocytes. To determine the most influential

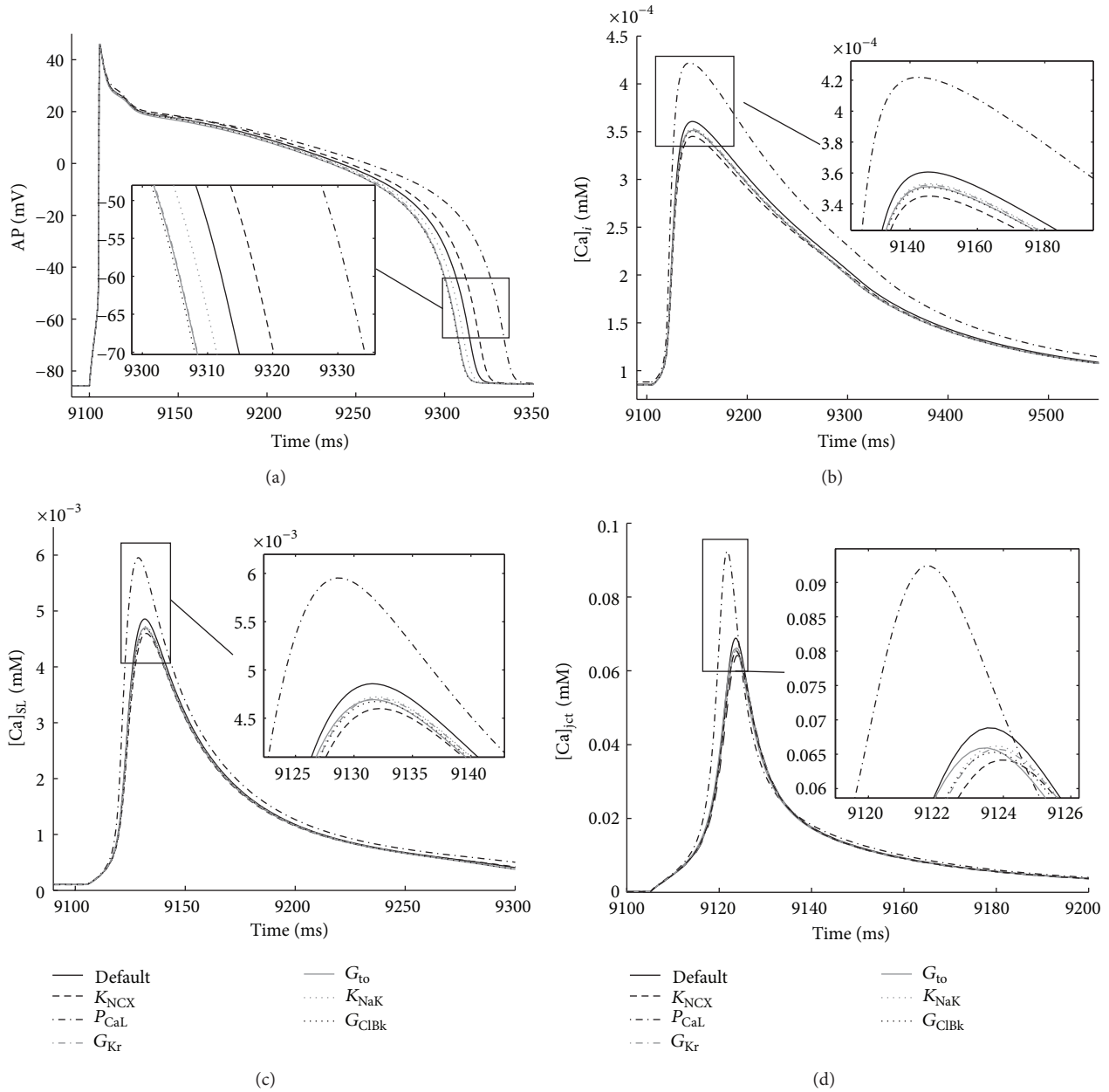


FIGURE 3: Verification of ion conductance sensitivity predictions. Steady-state AP and Ca^{2+} transients (recorded 9-10 s) in each of the three non-SR compartments in response to 1 Hz stimulus. The predicted changes in APD_{60} and Ca^{2+} peaks (see *Insets* also) are consistent with the generated by Nimrod/E and PLS outputs with respect to 10% increases in transporters' conductance. Control conductance values (black solid line) and 10% increases in K_{NCX} (black dashed line), P_{CaL} (black dash-dot line), G_{Kr} (gray dash-dot line), G_{to} (gray solid line), K_{NaK} (gray dotted line), and G_{CIBk} (black dotted line).

parameters controlling underlying subcellular mechanisms, we applied and compared the outcomes from two sensitivity analysis toolkits (PLS and Nimrod). The sensitivity of selected biomarkers (APD_{60} , $\Delta[Ca]_i$, $\Delta[Ca]_{st}$, and $\Delta[Ca]_{jct}$) to the alterations in ionic currents' properties and intracellular ionic transport was quantified using the Shannon et al. ionic model in rabbit ventricular cells, the predictive power of which has been demonstrated previously [1, 2].

4.1. Effects of Small Variations in Ionic Currents on AP Duration and Ca^{2+} Transients. Using parameter sensitive analysis,

Romero et al. quantified the sensitivity of AP properties, Ca^{2+} and Na^+ dynamics, and their rate dependence with respect to $\pm 15\%$, $\pm 30\%$, $\pm 45\%$, and $\pm 100\%$ variations in the main transmembrane currents' conductance [9]. It remains, however, poorly understood how *small variations* ($\pm 5\%$, $\pm 10\%$) in ion currents conductance affect cellular biomarkers. Our next studies contribute to filling up this knowledge gap further. Analysis suggests that the selected biomarkers were strongly dependent on I_{Ca} current properties. Results indicate that 10% increase in maximal permeability of L-type Ca^{2+} channel (P_{CaL}), with respect to other currents' conductance changes,

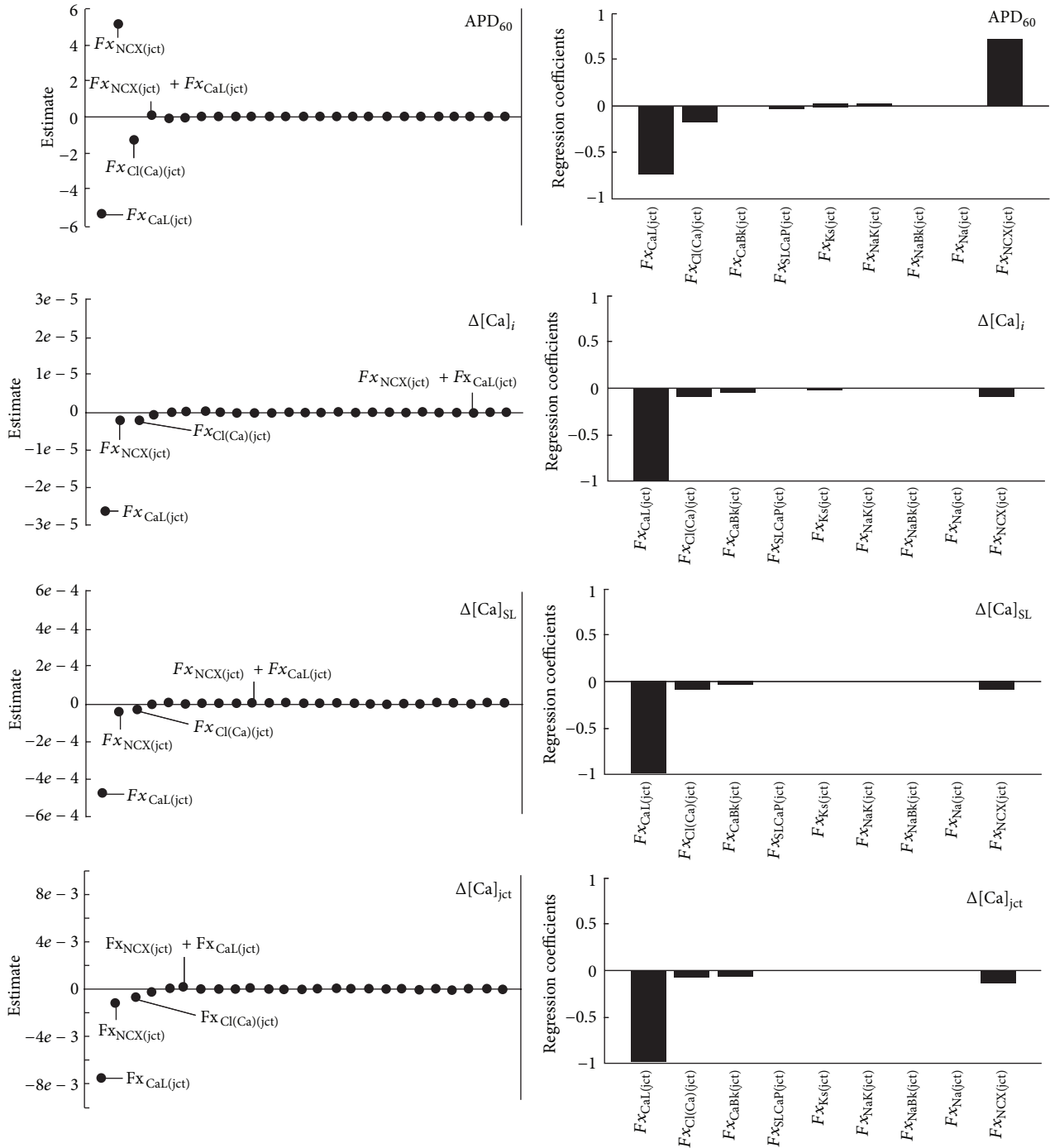


FIGURE 4: Parameter sensitivity analysis of APD_{60} , $\Delta[Ca]_i$, $\Delta[Ca]_{SL}$, and $\Delta[Ca]_{jct}$ sensitivities toward 5% increases in ion transporter distributions in the junctional cleft. Transporters' distribution between sarcolemma and junctional cleft summed up to 100%. Increasing fraction of total j -current in the junction by 5% is analogous to decreasing fraction of total j -current in the subsarcolemma by 45% for I_{Ca} and by 40-41% for all other currents. Positive value indicates direct relationship between distribution and output (e.g., increased density of I_{Ca} in the junctional cleft shortens APD_{60}) and negative value indicates indirect relationship between parameter and output. Nimrod/E-Lenth plots (left column), PLS-bar plots (right column). Nimrod/E analysis produced similar qualitative results as PLS analysis.

most notably affected APD_{60} and Ca^{2+} transients' peaks at 1Hz. Our predictions for the effects of P_{CaL} on APD and cytosolic Ca^{2+} peak are also consistent with reported data in rabbit ventricular myocytes after applications of I_{Ca} blockers

[5, 9, 29] or in cells with high L-type Ca^{2+} channel density [30]. The effects of 10% increase in G_{Kr} , G_{to} , K_{NCX} , or K_{NaK} on cellular biomarkers, while less pronounced than P_{CaL} , were still detectible. Our predictions for K_{NCX} increase at 1Hz

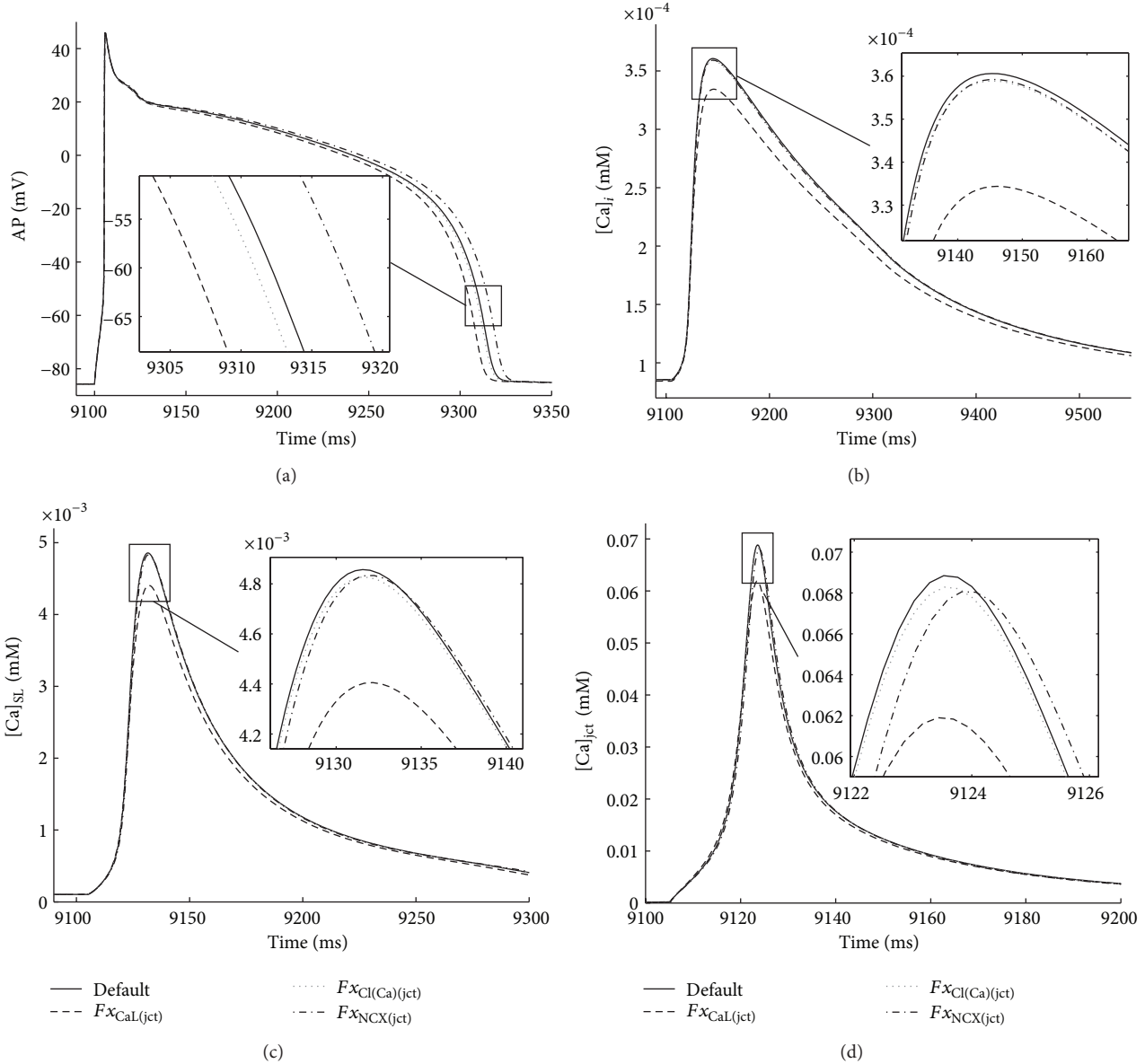


FIGURE 5: Verification of transporter distribution sensitivity predictions. Steady-state model outputs (recorded 9-10 s) in response to 1 Hz periodic pulse. The predicted alterations in APD_{60} and Ca^{2+} peaks (see *Insets* also) are consistent with the generated by Nimrod/E and PLS results with respect to 5% increases in transporters' fraction in the junctional cleft. Default j -currents' fractions in junctional cleft (black solid line) and 5% increases in $Fx_{CaL(jct)}$ (black dashed line), $Fx_{Cl(Ca)(jct)}$ (grey dotted line), $Fx_{NCX(jct)}$ (black dash-dot line).

are in qualitative agreement with data in ferret myocytes [31] and data supporting APD prolongation following I_{NCX} block reported in some experiments in rabbit cardiomyocytes [32, 33]. Several studies in rabbit ventricular cells report also a strong effect of I_{NCX} in modulating systolic $[Ca]_i$ transient [31–34] while others report only a moderate effect [35], similar to our predictions for $\Delta[Ca]_i$. Results demonstrate also that 10% increase in K_{NCX} slightly decreased $[Ca]_{jct}$ and $[Ca]_{SL}$ peaks. Increase in G_{Kr} and G_{to} at 1 Hz resulted in APD shortening, which is consistent with experiments in rabbit ventricular myocytes [36, 37]. Important role of I_{to} in modulating Ca^{2+} transients through its effects on I_{Ca} and

I_{NCX} during AP repolarization period has been suggested [38, 39]. Slight effects, however, due to 10% increase in G_{to} at 1 Hz on Ca^{2+} peaks are predicted here. Furthermore, at stimulus frequency of 2.5 Hz, Romero et al. report I_{NaK} ($\pm 30\%$ changes or severe I_{NaK} block; 0–8 min) as important influent current in most simulated cellular biomarkers, including APD_{60} [9]. Our studies quantitatively confirmed Romero et al. findings at 2.5 Hz (data not shown). At 1 Hz, however, the effect of $\pm 30\%$ changes in K_{NaK} (increment 5%, 0–8 min) on APD_{60} was less pronounced. The main reason for this observation was that the predicted changes in $[Na]_i$ were smaller at 1 Hz (20–100 μM) versus 1–1.5 mM at 2.5 Hz, in this way affecting

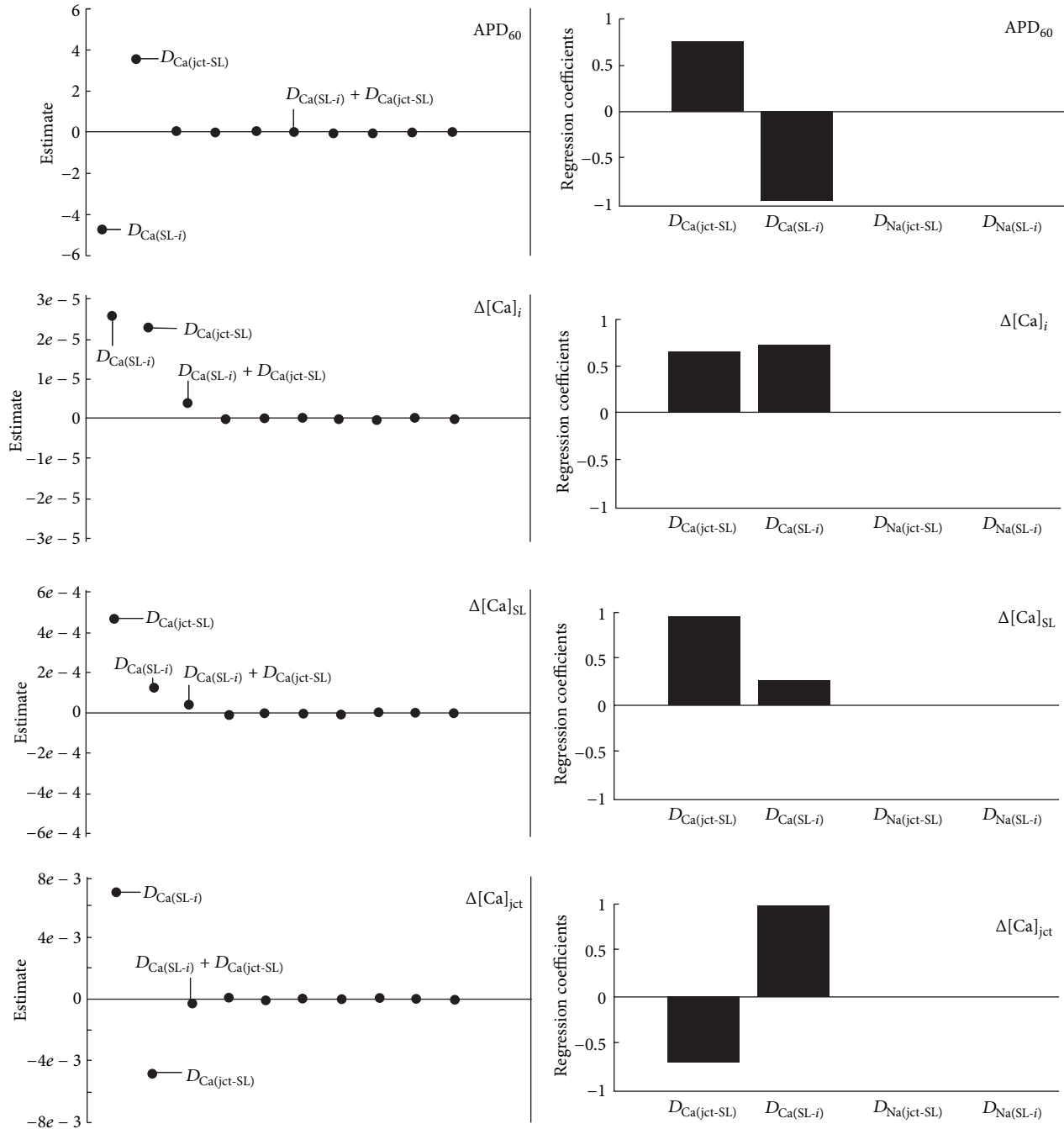


FIGURE 6: Parameter sensitivity analysis of APD_{60} , $\Delta[Ca]_i$, $\Delta[Ca]_{SL}$, and $\Delta[Ca]_{jct}$ sensitivities toward 10% increases in Ca^{2+} and Na^+ diffusion coefficients between subcellular compartments. Positive value indicates direct relationship between diffusion coefficient and output (e.g., increased diffusion coefficient between junctional cleft and sarcolemma prolongs APD_{60}) and negative sensitivity value indicates indirect relationship between parameter and output. Nimrod/E-Lenth plots (left column), PLS-bar plots (right column). Nimrod/E analysis produced similar qualitative results as PLS analysis.

differently I_{NaK} and I_{NCX} activities. These results indicate that the stimulus frequency is important factor regulating the electrophysiological biomarkers. Accordingly, because the Shannon et al. model mimics rabbit electrophysiology more accurately at normal pacing rates of 1 Hz [9], the model predictions for the effects of changes of ion current conductivities at faster rates should be considered with caution.

Interestingly, 10% increase in Cl^- background current (I_{ClBk}), which is a new feature of the Shannon et al. model, showed a negative relationships with four outputs (APD_{60} , $\Delta[Ca]_i$, $\Delta[Ca]_{SL}$, and $\Delta[Ca]_{jct}$) of approximately similar magnitude as for G_{to} or G_{Kr} . Experimental data reporting the effects of I_{ClBk} on rabbit ECC are missing in the literature however. Another interesting finding is the relatively small sensitivity

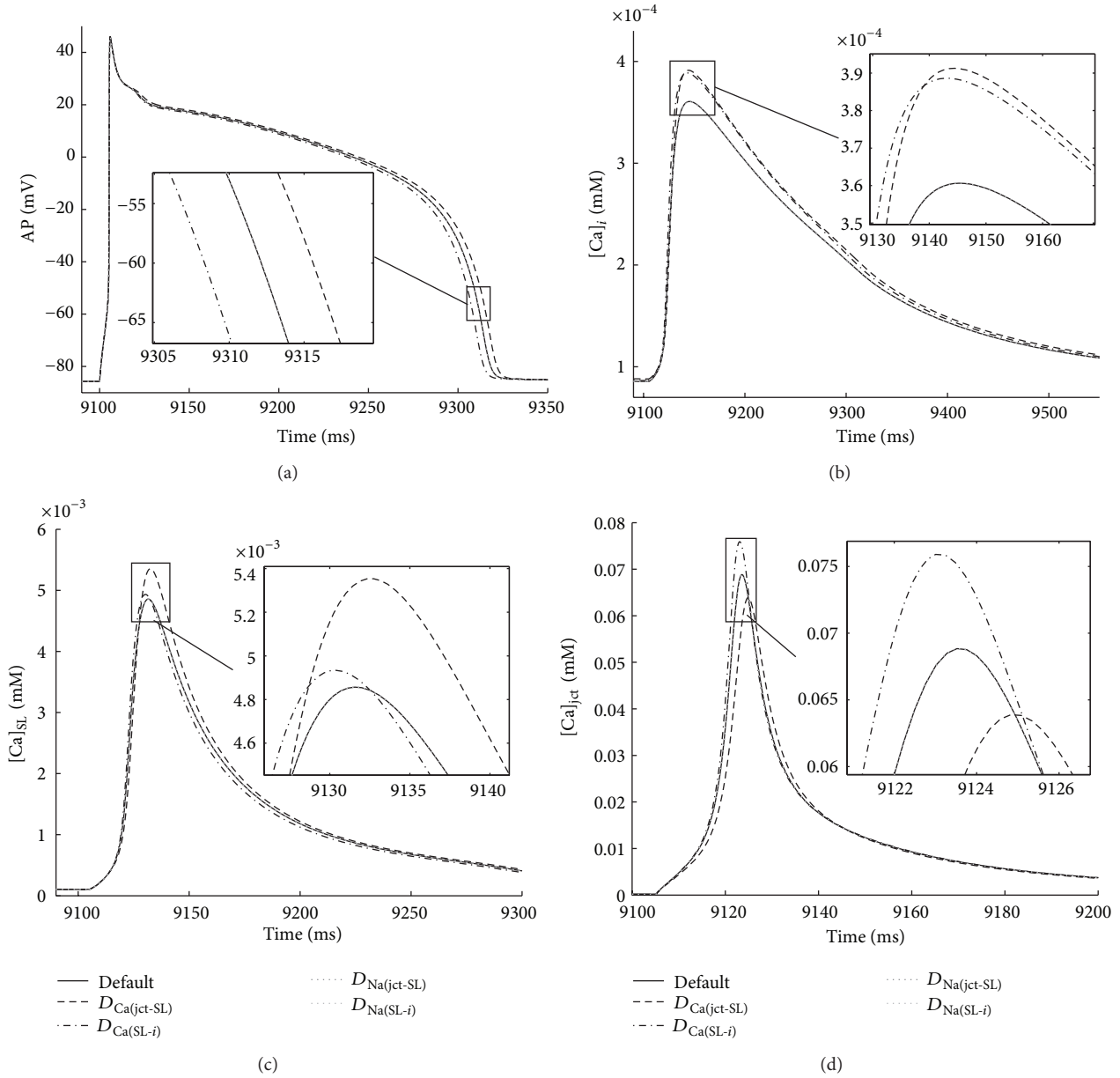


FIGURE 7: Verification of Ca^{2+} and Na^{+} diffusion sensitivity predictions. Steady-state AP and Ca^{2+} transients (recorded 9-10 s) in three non-SR compartments in response to 1Hz stimulus. The relative changes in APD_{60} and Ca^{2+} peaks (see *Insets* also) are consistent with predictions generated by Nimrod/E and PLS with respect to 10% increases in Ca^{2+} and Na^{+} diffusion constants. Control diffusion coefficients (black solid line) and 10% increases in $D_{\text{Ca}(\text{jct-SL})}$ (black dashed line), $D_{\text{Ca}(\text{SL-i})}$ (black dash-dot line), $D_{\text{Na}(\text{jct-SL})}$ (gray dotted lines), $D_{\text{Na}(\text{SL-i})}$ (light gray dotted lines).

of the biomarkers to 10% increases in G_{Na} , $G_{\text{Na,b}}$, P_{CaK} , P_{CaNa} , $G_{\text{Ca,b}}$, $G_{\text{to,f}}$, G_{Ks} , G_{K1} , $G_{\text{Cl}(\text{Ca})}$, K_{rel} , K_{leak} , K_{up} , and K_{pCa} factors at 1Hz. Thus, to further test the predictive power of the Shannon et al. model we examined the effects of severe currents' and SR-fluxes' block (up to 100%) (data not shown). In qualitative agreement with experiment [9] our studies show that (1) APD_{60} was highly sensitive to 100% I_{Na} , I_{K1} , K_{rel} , and K_{up} and block and less sensitive to I_{CaK} , $I_{\text{Cl}(\text{Ca})}$, $I_{\text{to,f}}$, and I_{pCa} inhibition while 100% block of $I_{\text{Na,b}}$, I_{CaNa} , $I_{\text{Ca,b}}$, and I_{Ks} currents and SR Ca^{2+} leak (K_{leak}) had small or

no effect; (2) steady-state Ca^{2+} peaks were strongly affected when I_{Na} , $I_{\text{Ca,b}}$, and SR Ca^{2+} fluxes (K_{rel} , K_{leak} , and K_{up}) were inhibited whereas 100% block I_{pCa} , $I_{\text{Cl}(\text{Ca})}$, I_{CaK} , I_{K1} , and $I_{\text{to,f}}$ had less pronounced effects. New measurements in rabbit ventricular myocytes are needed to define the relative importance of G_{Na} , $G_{\text{Na,b}}$, P_{CaK} , P_{CaNa} , $G_{\text{Ca,b}}$, $G_{\text{to,f}}$, G_{Ks} , G_{K1} , $G_{\text{Cl}(\text{Ca})}$, K_{rel} , K_{leak} , K_{up} , and K_{pCa} in determining physiological responses due to the small changes in these factors at 1 Hz and to test further the capabilities and limitations of the Shannon et al. model. Using Nimrod/E, we also examined

how simultaneous changes in two transmembrane currents affect APD and Ca^{2+} dynamics. Our analysis suggests that 10% increase in both P_{CaL} and K_{NCX} had minor effect at 1 Hz. Additionally, Nimrod/E showed that simultaneous increases in control I_{Ca} and K^+ related currents had slight or no effect (data not shown). Furthermore, the predicted effects of $\pm 5\%$ changes in channels conductance were identical to those with $\pm 10\%$ variations (data not shown). Such insights, coming from mathematical models, might be useful in searching new avenues for development of methodologies to predict drug action effects on behavior of cardiac cells. For example, most I_{Ca} inhibitors suppress partially K^+ -related currents also; therefore the balance of these currents is critical for predicting I_{Ca} -related drug action.

4.2. Effects of Variations in Membrane Transporters Distribution on AP Duration and Ca^{2+} Transients. Experimental studies have demonstrated that in rabbit ventricular myocytes marked variations in the distribution of ion transports along the surface membrane probably exist [1, 40–42]. Using reaction-diffusion models, recently we demonstrated that the subcellular Ca^{2+} signals are highly sensitive to I_{Ca} and I_{NCX} fluxes distributions via the sarcolemma [13, 16, 19, 20]. In these spatial models, however, the cell electrophysiology was simplified; equations describing I_{Ca} , I_{NCX} , I_{pCa} , and $I_{\text{Ca,b}}$ properties were only included; and AP dynamics were not reproduced. Additionally, *small variations* in L-type Ca^{2+} channels density in junctional cleft have been suggested to lead to large changes in control SR Ca^{2+} release, subcellular Ca^{2+} transients, and AP waveform [4, 5]. Thus, we used PLS and Nimrod/E to gain further insights into how $\pm 5\%$ changes in L-type and other ion transporters' distributions influence control AP and Ca^{2+} transients. We evaluated the biomarkers' sensitivity to 5% increases in the fraction of total ionic current in the junctional cleft ($Fx_{j(\text{ct})}$) assuming total number of transporters within the sarcolemma unchanged; that is, $Fx_{j(\text{ct})} + Fx_{j(\text{SL})} = 1$. Our results yielded three channel distributions ($Fx_{\text{CaL}(j(\text{ct}))}$, $x_{\text{NCX}(j(\text{ct}))}$, and $Fx_{\text{Cl}(\text{Ca})(j(\text{ct}))}$) that significantly affect the model outcomes of interest (i.e., APD_{60} , $\Delta[\text{Ca}]_i$, $\Delta[\text{Ca}]_{\text{SL}}$, and $\Delta[\text{Ca}]_{\text{jct}}$). Increasing by 5% the density of L-type Ca^{2+} channels in the junctional cleft (while decreasing by 45% I_{Ca} density in SL compartment to keep $Fx_{\text{CaL}(j(\text{ct}))} + Fx_{\text{CaL}(\text{SL})} = 1$) had the strongest effect on both APD_{60} and Ca^{2+} peaks, decreasing APD_{60} and $[\text{Ca}]_i$, $[\text{Ca}]_{\text{SL}}$, and $[\text{Ca}]_{\text{jct}}$ peaks. The reason for the predicted decrease in $[\text{Ca}]_{\text{jct}}$ was the strongly increased rate of Ca^{2+} transfer from the junctional cleft to the submembrane space evoked by the 5% increase of $Fx_{\text{CaL}(j(\text{ct}))}$ and reduced I_{Ca} ($\sim 45\%$) into the SL compartment. The predicted decreases into $[\text{Ca}]_{\text{SL}}$ peak and APD_{60} were also consequence of $Fx_{\text{CaL}(\text{SL})}$ reduction to 45% though Ca^{2+} flux from the cleft was increased. The drop in $[\text{Ca}]_{\text{SL}}$ evoked decrease in the rate of Ca^{2+} transfer from the SL to cytosolic compartment thus causing drop in $[\text{Ca}]_i$ peak as well. Our studies also showed that the effects of I_{NCX} redistribution were quite different. The 5% increase in $Fx_{\text{NCX}(j(\text{ct}))}$ (while decreasing by 40–41% I_{NCX} density in SL

compartment to keep $Fx_{\text{NCX}(j(\text{ct}))} + Fx_{\text{NCX}(\text{SL})} = 1$) prolonged APD_{60} to approximately the same magnitude as for I_{Ca} and slightly decreased the control Ca^{2+} peaks. Significant effects due to I_{Ca} redistribution and negligible effects due to I_{NCX} redistribution on the local and global Ca^{2+} transients' peaks were also found using our reaction-diffusion model in rabbit ventricular cells [20]. Calcium activated chloride current ($I_{\text{Cl}(\text{Ca})}$) has been extensively studied [43–45]. Experimental data in rabbit ventricular myocytes suggest that $I_{\text{Cl}(\text{Ca})}$ is strongly temperature dependent (very small at room temperature but substantial at 35°C – 37°C); $I_{\text{Cl}(\text{Ca})}$ can be eliminated by blocking I_{Ca} ; and $I_{\text{Cl}(\text{Ca})}$ may normally facilitate rapid repolarization when SR Ca^{2+} load and release are high. To bring further insights into the effects of $I_{\text{Cl}(\text{Ca})}$ properties on ECC, we examined how 5% increase in $I_{\text{Cl}(\text{Ca})}$ density in the junctional cleft (assuming $Fx_{\text{Cl}(\text{Ca})(j(\text{ct}))} + Fx_{\text{Cl}(\text{Ca})(\text{SL})} = 1$) may affect the cell electrical activity and Ca^{2+} signaling. Interestingly, although much less pronounced than $Fx_{\text{CaL}(j(\text{ct}))}$ variations, changes in $Fx_{\text{Cl}(\text{Ca})(j(\text{ct}))}$ were able also to shorten APD_{60} and provide negative feedback on cell Ca^{2+} load. Negligible effects due to 5% increases in I_{Na} , $I_{\text{Na,b}}$, I_{NaK} , I_{Ks} , $I_{\text{Ca,b}}$, and I_{pCa} currents' fractions in the junctional cleft were found. Finally, Nimrod/E predicted slight or no effect on model outputs when $Fx_{\text{CaL}(j(\text{ct}))}$ and $Fx_{\text{NCX}(j(\text{ct}))}$, or any other two-parameter $Fx_{j(\text{ct})}$ groups, were combined. These model studies imply that more accurate experimental knowledge of I_{Ca} , $I_{\text{Cl}(\text{Ca})}$ and I_{NCX} fluxes distributions is needed to better understand the physiological role of $I_{\text{Cl}(\text{Ca})}$ current, the local Ca^{2+} signaling, and the electrical cell activity. Furthermore, the estimates of % total flux in junctional cleft versus submembrane space under control conditions are still under debate. Additional quantification of the model sensitivity to $\pm 10\%$ changes in $Fx_{\text{CaL}(j(\text{ct}))}$ or $\pm 10\%$ and $\pm 15\%$ variations in other transporters' densities in the cleft (not done in this study) may provide a more convincing conclusions.

4.3. Effects of Small Variations in Intracellular Ion Transport on AP Duration and Ca^{2+} Transients. In the Shannon et al. model the diffusion of Ca^{2+} and Na^+ ions was considered where (1) the junctional compartment communicates only with the SL compartment, (2) the SL compartment with the junctional and the bulk cytosolic compartments, and (3) the bulk cytosolic compartment only with the SL compartment. The values of the effective diffusion coefficients for Ca^{2+} and Na^{2+} were average values measured in different cardiac tissues and species under control conditions. In the literature, however, these estimates are contradictable [1, 8, 10–20]. In this study, we tested how *small changes* (± 5 , $\pm 10\%$) in suggested diffusion coefficients may influence the model outputs. We used PLS and Nimrod toolkits to determine the most influential ion diffusion parameter(s) governing the properties of the electrical signal (such as APD_{60}) and of the Ca^{2+} signal (such as peak level of Ca^{2+} transient in the junctional cleft, subsarcolemmal space, and bulk cytosol). While 10% increases in basal Ca^{2+} diffusion coefficients ($D_{\text{Ca}(j(\text{ct}-\text{SL})}$ and $D_{\text{Ca}(\text{SL}-i)}$) had pronounced effects on the model

outputs, no visible changes in all selected biomarkers were detected due to 10% increases in Na^+ diffusion coefficients ($D_{\text{Na}(\text{jct-SL})}$ and $D_{\text{Na}(\text{SL-i})}$). Interestingly marked effects on both APD_{60} and Ca^{2+} peaks were predicted when Na^+ diffusion was blocked, assuming $D_{\text{Na}(\text{jct-SL})}$ and $D_{\text{Na}(\text{SL-i})}$ zeros shorten APD_{60} and decreased $[\text{Ca}]_i$, $[\text{Ca}]_{\text{SL}}$, and $[\text{Ca}]_{\text{jct}}$ peaks (data not shown). Our results also demonstrate that accelerating Ca^{2+} transfer from junctional to submembrane space (e.g., increasing $D_{\text{Ca}(\text{jct-SL})}$), (1) sensitively decreased Ca^{2+} peak in the junctional cleft and prolonged $[\text{Ca}]_{\text{jct}}$ time to peak, (2) enhanced $[\text{Ca}]_{\text{SL}}$ and $[\text{Ca}]_i$ peaks, and (3) prolonged APD_{60} . The effects of $D_{\text{Ca}(\text{SL-i})}$ increase were quite different. Accelerating Ca^{2+} transfer from the SL compartment to the bulk cytosol (e.g., increasing $D_{\text{Ca}(\text{SL-i})}$) shortened APD_{60} and enhanced all Ca^{2+} transients' peaks. In addition, $D_{\text{Ca}(\text{SL-i})}$ increase most significantly enhanced $[\text{Ca}]_{\text{jct}}$ peak while the control $[\text{Ca}]_{\text{SL}}$ peak was less affected. Possible reason for the predicted increase in $[\text{Ca}]_{\text{jct}}$ peak, due to $D_{\text{Ca}(\text{SL-i})}$ increase, was enhanced $[\text{Ca}]_i$ which promoted increase in the SR load (i.e., $[\text{Ca}]_{\text{SR}}$) in this way causing additional Ca^{2+} release from the SR and consequent elevations in $[\text{Ca}]_{\text{jct}}$ and $[\text{Ca}]_{\text{SL}}$, respectively. The enhanced $[\text{Ca}]_{\text{SL}}$ transient produced faster Ca^{2+} -dependent inactivation of I_{Ca} , thus leading to APD shortening. Nimrod/E showed also that simultaneous increases in control $D_{\text{Ca}(\text{jct-SL})}$ and $D_{\text{Ca}(\text{SL-i})}$ slightly increased $\Delta[\text{Ca}]_i$ while all other biomarkers remained insensitive to the changes in any other two-level parameter combinations. Also predicted relative effects of $\pm 5\%$ changes in intracellular ion transport were identical to those of $\pm 10\%$ variations (data not shown). In summary, our results reveal that small variations in diffusion coefficients for Ca^{2+} may impact sensitively the cell electrical activity and Ca^{2+} homeostasis. New and more precise estimates of the effective Ca^{2+} and Na^+ diffusion constants are needed to better understand ECC in rabbit ventricular myocytes under control and certain pathologies.

We need to acknowledge that although we demonstrated good correlation with experiment, the results of sensitivity analysis strongly depend on the model details and simplifications. For example, in the lumped Shannon et al. model the ionic diffusion from junctional cleft to cytosolic compartment goes solely through subsarcolemmal space which is questionable with regard to the contact areas between these compartments [19]. In addition, in all studied cases the variations of intracellular potassium concentration were disabled (i.e., $d[\text{K}]_i/dt = 0$ in Shannon's MatLab code) and whether or not this drawback was eliminated in the Romero's code or in recent modifications of the Shannon's code is unclear [4–7, 9]. This limitation led to the following: (1) fast stabilisation of the model for $[\text{Ca}]_i$ and AP (after 6–8 s until 8 min); (2) $[\text{Na}]_i$ appeared stable after ~200 s; (3) diastolic $[\text{K}]_i$ remained unchanged in the interval $0 \leq t \leq 8$ min. Thus, models neglecting slow intracellular concentration changes in $[\text{K}]_i$ produced mainly by Na/K pump need to be revised further. Finally, the t -tubule compartment, the ion diffusion between the t -tubule lumen and bulk extracellular space, and the mitochondrial Ca^{2+} fluxes were omitted [46–50]. These are likely to have important impact on predicted AP and Ca^{2+} profiles as well.

5. Conclusions

Our studies demonstrate that parameter sensitivity approaches can be used to obtain new insights into relationships between model parameters, model outputs, and experimental data. More specifically, the simulation results provided information on how small variations in the ionic currents and intracellular Ca^{2+} and Na^+ diffusion modulate ventricular myocyte electrophysiology and Ca^{2+} dynamics in rabbit ventricular myocytes at 1 Hz. We found that APD_{60} and Ca^{2+} peaks are (1) highly sensitive to 10% increase in I_{Ca} , while the effects of I_{NCX} , I_{NaK} , I_{Kr} , I_{to} , and I_{ClBk} were moderate, and (2) insensitive to 10% increases in all other Ca^{2+} , Na^+ , and K^+ transmembrane currents and SR Ca^{2+} fluxes. The myocyte electrical activity is highly sensitive to 5% variations in I_{Ca} and I_{NCX} and less sensitive to $I_{\text{Cl}(\text{Ca})}$ redistribution between junctional cleft and submembrane space. Small changes in submembrane and cytosolic diffusion coefficients for Ca^{2+} , but not in Na^+ diffusion coefficients, may impact notably the myocyte contraction. This study highlights the need for additional and more precise experimental data and further updating and testing of the Shannon et al. model and its recent modifications to fill specific knowledge gaps related to rabbit ventricular electrophysiology and intracellular Ca^{2+} signaling.

Appendix

See Tables 1, 2, and 3.

Glossary

Abbreviations

ECC:	Excitation-contraction coupling
AP:	Action potential
APD_{60} :	Action potential duration at 60% repolarization
SL:	Sarcolemmal membrane
SR:	Sarcoplasmic reticulum
RyR:	Ryanodine receptor
SERCA2:	SR Ca^{2+} ATPase pump
TnC:	Troponin C
NIMROD:	Parameter modeling toolkit for sensitivity analysis
PLS:	Partial least square tool.

Membrane Currents

I_{Na} :	Na^+ current
$I_{\text{Na,b}}$ (I_{NaBk}):	Na^+ background current
I_{Ca} (I_{CaL}):	L-type Ca^{2+} channel current
$I_{\text{Ca,b}}$ (I_{CaBk}):	Ca^{2+} background current
$I_{\text{to,f}}$:	Fast transient outward K^+ current
I_{to} ($I_{\text{to,s}}$):	Slow transient outward K^+ current
I_{Kr} :	Rapid delayed rectifier K^+ current
I_{Ks} :	Slow delayed rectifier K^+ current

I_{K1} :	Inward rectifier K^+ current
$I_{Cl(Ca)}$:	Ca^{2+} activated Cl^- current
I_{ClBk} :	Cl^- background current
I_{NaK} :	Na^+ - K^+ pump current
I_{NCX} :	Na^+ - Ca^{2+} exchanger current
I_{pCa} (I_{SLCaP}):	Sarcolemmal Ca^{2+} pump current.

Concentrations

$[Ca]_i$:	Cytosolic Ca^{2+} concentration
$[Ca]_{SL}$:	Subsarcolemmal Ca^{2+} concentration
$[Ca]_{jct}$:	Junctional cleft Ca^{2+} concentration
$[Ca]_{SR}$:	SR Ca^{2+} concentration
$[Na]_i$:	Cytosolic Na^+ concentration
$[K]_i$:	Cytosolic K^+ concentration.

Acknowledgments

The authors thank Dr. Jiří Šimurda for helpful suggestions and careful reading of the paper. This work is supported by NIBIB 1R03EB014593-01 (Michailova), National Biomedical Computational Resource (NIH grant 8P41 GM103426-19), NHLBI Systems Biology Collaboration 1R01HL105242-01 (McCulloch), and NSF funded PRIME program (NSF grant IOSE 0710726).

References

- [1] T. R. Shannon, F. Wang, J. Puglisi, C. Weber, and D. M. Bers, "A mathematical treatment of integrated Ca dynamics within the ventricular myocyte," *Biophysical Journal*, vol. 87, no. 5, pp. 3351–3371, 2004.
- [2] T. R. Shannon, F. Wang, and D. M. Bers, "Regulation of cardiac sarcoplasmic reticulum Ca release by luminal [Ca] and altered gating assessed with a mathematical model," *Biophysical Journal*, vol. 89, no. 6, pp. 4096–4110, 2005.
- [3] J. L. Puglisi and D. M. Bers, "LabHEART: an interactive computer model of rabbit ventricular myocyte ion channels and Ca transport," *American Journal of Physiology: Cell Physiology*, vol. 281, no. 6, pp. C2049–C2060, 2001.
- [4] A. Mahajan, Y. Shiferaw, D. Sato et al., "A rabbit ventricular action potential model replicating cardiac dynamics at rapid heart rates," *Biophysical Journal*, vol. 94, no. 2, pp. 392–410, 2008.
- [5] A. Mahajan, D. Sato, Y. Shiferaw et al., "Modifying L-type calcium current kinetics: consequences for cardiac excitation and arrhythmia dynamics," *Biophysical Journal*, vol. 94, no. 2, pp. 411–423, 2008.
- [6] O. V. Aslanidi, R. N. Sleiman, M. R. Boyett, J. C. Hancox, and H. Zhang, "Ionic mechanisms for electrical heterogeneity between rabbit Purkinje fiber and ventricular cells," *Biophysical Journal*, vol. 98, no. 11, pp. 2420–2431, 2010.
- [7] S. Morotti, E. Grandi, A. Summa, K. S. Ginsburg, and D. M. Bers, "Theoretical study of L-type Ca^{2+} current inactivation kinetics during action potential repolarization and early afterdepolarizations," *The Journal of Physiology*, vol. 590, part 18, pp. 4465–4481, 2012.
- [8] M. S. Jafri, J. J. Rice, and R. L. Winslow, "Cardiac Ca^{2+} dynamics: the roles of ryanodine receptor adaptation and sarcoplasmic reticulum load," *Biophysical Journal*, vol. 74, no. 3, pp. 1149–1168, 1998.
- [9] L. Romero, B. Carbonell, B. Trenor, B. Rodríguez, J. Saiz, and J. M. Ferrero, "Systematic characterization of the ionic basis of rabbit cellular electrophysiology using two ventricular models," *Progress in Biophysics and Molecular Biology*, vol. 107, no. 1, pp. 60–73, 2011.
- [10] M. B. Cannell and D. G. Allen, "Model of calcium movements during activation in the sarcomere of frog skeletal muscle," *Biophysical Journal*, vol. 45, no. 5, pp. 913–925, 1984.
- [11] G. A. Langer and A. Peskoff, "Calcium concentration and movement in the diadic cleft space of the cardiac ventricular cell," *Biophysical Journal*, vol. 70, no. 3, pp. 1169–1182, 1996.
- [12] A. Michailova, F. DelPrincipe, M. Egger, and E. Niggli, "Spatiotemporal features of Ca^{2+} buffering and diffusion in atrial cardiac myocytes with inhibited sarcoplasmic reticulum," *Biophysical Journal*, vol. 83, no. 6, pp. 3134–3151, 2002.
- [13] S. Lu, A. Michailova, J. J. Saucerman et al., "Multi-scale modeling in rodent ventricular myocytes: contributions of structural and functional heterogeneities to excitation-contraction coupling," *IEEE Engineering in Medicine and Biology Magazine*, vol. 28, no. 2, pp. 46–57, 2009.
- [14] L. T. Izu, S. A. Means, J. N. Shadid, Y. Chen-Izu, and C. W. Balke, "Interplay of ryanodine receptor distribution and calcium dynamics," *Biophysical Journal*, vol. 91, no. 1, pp. 95–112, 2006.
- [15] S. Means, A. J. Smith, J. Shepherd et al., "Reaction diffusion modeling of calcium dynamics with realistic ER geometry," *Biophysical Journal*, vol. 91, no. 2, pp. 537–557, 2006.
- [16] Y. Cheng, Z. Yu, M. Hoshijima et al., "Numerical analysis of Ca^{2+} signaling in rat ventricular myocytes with realistic transverse-axial tubular geometry and inhibited sarcoplasmic reticulum," *PLoS Computational Biology*, vol. 6, no. 10, Article ID 1000972, 2010.
- [17] A. Hatano, J.-I. Okada, T. Washio, T. Hisada, and S. Sugiura, "A three-dimensional simulation model of cardiomyocyte integrating excitation-contraction coupling and metabolism," *Biophysical Journal*, vol. 101, no. 11, pp. 2601–2610, 2011.
- [18] A. Hatano, J.-I. Okada, T. Hisada, and S. Sugiura, "Critical role of cardiac t-tubule system for the maintenance of contractile function revealed by a 3D integrated model of cardiomyocytes," *Journal of Biomechanics*, vol. 45, no. 5, pp. 815–823, 2012.
- [19] J. E. Hake, A. G. Edwards, Z. Yu et al., "Modeling cardiac calcium sparks in a three-dimensional reconstruction of a calcium release unit," *The Journal of Physiology*, vol. 590, no. 18, pp. 4403–4422, 2012.
- [20] P. M. Kekenus-Huskey, Y. Cheng, J. E. Hake et al., "Modeling effects of L-type Ca^{2+} current and Na^+ - Ca^{2+} exchanger on Ca^{2+} trigger flux in rabbit myocytes with realistic T-tubule geometries," *Frontiers in Physiology*, vol. 3, article 351, 2012.
- [21] M. Fink and D. Noble, "Markov models for ion channels: versatility versus identifiability and speed," *Philosophical Transactions of the Royal Society A*, vol. 367, no. 1896, pp. 2161–2179, 2009.
- [22] E. A. Sobie, "Parameter sensitivity analysis in electrophysiological models using multivariable regression," *Biophysical Journal*, vol. 96, no. 4, pp. 1264–1274, 2009.
- [23] M. D. Moris, "Factorial sampling plans for preliminary computational experiments," *Technometrics*, vol. 33, pp. 161–174, 1991.
- [24] D. Abramson, R. Sosic, J. Giddy, and B. Hall, "Nimrod: a tool for performing parametrised simulations using distributed workstations," in *Proceedings of the 4th IEEE International Symposium*

- on *High Performance Distributed Computing (HPDC '95)*, pp. 112–121, Pentagon City, Va, USA, August 1995.
- [25] H. Abdi, “Partial least squares (PLS) regression,” in *Encyclopedia of Measurements and Statistics*, N. J. Salkind, Ed., pp. 740–744, Sage, Thousand Oaks, Calif, USA, 2007.
- [26] D. Abramson, J. Giddy, and L. Kotler, “High performance parametric modeling with Nimrod/G: killer application for the global grid?” in *Proceedings of the 14th International Parallel and Distributed Processing Symposium (IPDPS '00)*, pp. 520–528, Cancun, Mexico, May 2000.
- [27] D. Abramson, A. Lewis, and T. Peachey, “Nimrod/O: a tool for automatic design optimization,” in *Proceedings of the 4th International Conference on Algorithms & Architectures for Parallel Processing (ICA3PP '00)*, World Scientific, Hong Kong, December 2000.
- [28] T. C. Peachey, N. T. Diamond, D. A. Abramson, W. Sudholt, A. Michailova, and S. Amirrazi, “Fractional factorial design for parameter sweep experiments using Nimrod/E,” *Scientific Programming*, vol. 16, no. 2-3, pp. 217–230, 2008.
- [29] H. R. Lu, E. Vlamincx, and D. J. Gallacher, “Choice of cardiac tissue in vitro plays an important role in assessing the risk of drug-induced cardiac arrhythmias in human: beyond QT prolongation,” *Journal of Pharmacological and Toxicological Methods*, vol. 57, no. 1, pp. 1–8, 2008.
- [30] C. Sims, S. Reisenweber, P. C. Viswanathan, B.-R. Choi, W. H. Walker, and G. Salama, “Sex, age, and regional differences in L-type calcium current are important determinants of arrhythmia phenotype in rabbit hearts with drug-induced long QT type 2,” *Circulation Research*, vol. 102, no. 9, pp. e86–e100, 2008.
- [31] A. Tóth, L. Kiss, A. Varró, and P. P. Nánási, “Potential therapeutic effects of $\text{Na}^+/\text{Ca}^{2+}$ exchanger inhibition in cardiac diseases,” *Current Medicinal Chemistry*, vol. 16, no. 25, pp. 3294–3321, 2009.
- [32] H. K. Ranu, C. M. N. Terracciano, K. Davia et al., “Effects of $\text{Na}^+/\text{Ca}^{2+}$ -exchanger overexpression on excitation-contraction coupling in adult rabbit ventricular myocytes,” *Journal of Molecular and Cellular Cardiology*, vol. 34, no. 4, pp. 389–400, 2002.
- [33] T. Seidler, S. L. W. Miller, C. M. Loughrey et al., “Effects of adenovirus-mediated sorcin overexpression on excitation-contraction coupling in isolated rabbit cardiomyocytes,” *Circulation Research*, vol. 93, no. 2, pp. 132–139, 2003.
- [34] W. Schillinger, P. M. L. Janssen, S. Emami et al., “Impaired contractile performance of cultured rabbit ventricular myocytes after adenoviral gene transfer of $\text{Na}^+-\text{Ca}^{2+}$ exchanger,” *Circulation Research*, vol. 87, no. 7, pp. 581–587, 2000.
- [35] A. S. Farkas, K. Acsai, N. Nagy et al., “ $\text{Na}^+/\text{Ca}^{2+}$ exchanger inhibition exerts a positive inotropic effect in the rat heart, but fails to influence the contractility of the rabbit heart,” *British Journal of Pharmacology*, vol. 154, no. 1, pp. 93–104, 2008.
- [36] D. Guo, J. Zhou, X. Zhao et al., “L-type calcium current recovery versus ventricular repolarization: preserved membrane-stabilizing mechanism for different QT intervals across species,” *Heart Rhythm*, vol. 5, no. 2, pp. 271–279, 2008.
- [37] C. L. Lawrence, M. H. Bridgland-Taylor, C. E. Pollard, T. G. Hammond, and J.-P. Valentin, “A rabbit Langendorff heart proarrhythmia model: predictive value for clinical identification of Torsades de Pointes,” *British Journal of Pharmacology*, vol. 149, no. 7, pp. 845–860, 2006.
- [38] R. Sah, R. J. Ramirez, G. Y. Oudit et al., “Regulation of cardiac excitation-contraction coupling by action potential repolarization: role of the transient outward potassium current (I_{to}),” *Journal of Physiology*, vol. 546, no. 1, pp. 5–18, 2003.
- [39] K. W. Linz and R. Meyer, “Profile and kinetics of L-type calcium current during the cardiac ventricular action potential compared in guinea-pigs, rats and rabbits,” *Pflügers Archiv*, vol. 439, no. 5, pp. 588–599, 2000.
- [40] D. R. L. Scriven, P. Dan, and E. D. W. Moore, “Distribution of proteins implicated in excitation-contraction coupling in rat ventricular myocytes,” *Biophysical Journal*, vol. 79, no. 5, pp. 2682–2691, 2000.
- [41] C. Gershome, E. Lin, H. Kashihara, L. Hove-Madsen, and G. F. Tibbits, “Colocalization of voltage-gated Na^+ channels with the $\text{Na}^+/\text{Ca}^{2+}$ exchanger in rabbit cardiomyocytes during development,” *American Journal of Physiology: Heart and Circulatory Physiology*, vol. 300, no. 1, pp. H300–H311, 2011.
- [42] F. B. Sachse, N. S. Torres, E. Savio-Galimberti et al., “Subcellular structures and function of myocytes impaired during heart failure are restored by cardiac resynchronization therapy,” *Circulation Research*, vol. 110, no. 4, pp. 588–597, 2012.
- [43] A. C. Zygmunt and W. R. Gibbons, “Calcium-activated chloride current in rabbit ventricular myocytes,” *Circulation Research*, vol. 68, no. 2, pp. 424–437, 1991.
- [44] S. Kawano, Y. Hirayama, and M. Hiraoka, “Activation mechanism of Ca^{2+} -sensitive transient outward current in rabbit ventricular myocytes,” *Journal of Physiology*, vol. 486, no. 3, pp. 593–604, 1995.
- [45] J. L. Puglisi, W. Yuan, J. W. Bassani, and D. M. Bers, “ Ca^{2+} influx through Ca^{2+} channels in rabbit ventricular myocytes during action potential clamp: influence of temperature,” *Circulation Research*, vol. 85, no. 6, pp. e7–e16, 1999.
- [46] M. Pásek, J. Šimurda, and C. H. Orchard, “Role of t-tubules in the control of trans-sarcolemmal ion flux and intracellular Ca^{2+} in a model of the rat cardiac ventricular myocyte,” *European Biophysics Journal*, vol. 41, no. 6, pp. 491–503, 2012.
- [47] R. K. Dash, F. Qi, and D. A. Beard, “A biophysically based mathematical model for the kinetics of mitochondrial calcium uniporter,” *Biophysical Journal*, vol. 96, no. 4, pp. 1318–1332, 2009.
- [48] R. K. Pradhan, D. A. Beard, and R. K. Dash, “A biophysically based mathematical model for the kinetics of mitochondrial $\text{Na}^+-\text{Ca}^{2+}$ antiporter,” *Biophysical Journal*, vol. 98, no. 2, pp. 218–230, 2010.
- [49] S. Cortassa and M. A. Aon, “Computational modeling of mitochondrial function,” *Methods in Molecular Biology*, vol. 810, pp. 311–326, 2012.
- [50] E. N. Dedkova and L. A. Blatter, “Measuring mitochondrial function in intact cardiac myocytes,” *Journal of Molecular and Cellular Cardiology*, vol. 52, no. 1, pp. 48–61, 2012.